Nano Research
2021, 14(10): 3509–3513
ISSN 1998-0124 CN 11-5974/O4
https://doi.org/10.1007/s12274-021-3561-2

Research Article

Sulfur-doped graphene anchoring of ultrafine Au_{25} nanoclusters for electrocatalysis

Mufan Li[1,3,§], Bei Zhang[1,§], Tao Cheng[5], Sunmoon Yu[2,3], Sheena Louisia[1,3], Chubai Chen[1], Shouping Chen[2], Stefano Cestellos-Blanco[2], William A. Goddard III[5], and Peidong Yang[1,2,3,4] (✉)

[1] *Department of Chemistry, University of California, Berkeley, California 94720, USA*
[2] *Department of Materials Science and Engineering, University of California, Berkeley, California 94720, USA*
[3] *Chemical Science Division, Lawrence Berkeley National Laboratory, Berkeley, California 94720, USA*
[4] *Kavli Energy NanoScience Institute, Berkeley, California 94720, USA*
[5] *Materials and Process Simulation Center, California Institute of Technology, Pasadena, California 91125, USA*
[§] *Mufan Li and Bei Zhang contributed equally to this work.*

Received: 20 February 2021 / **Revised:** 23 April 2021 / **Accepted:** 1 May 2021

ABSTRACT

The biggest challenge of exploring the catalytic properties of under-coordinated nanoclusters is the issue of stability. We demonstrate herein that chemical dopants on sulfur-doped graphene (S-G) can be utilized to stabilize ultrafine (sub-2 nm) $Au_{25}(PET)_{18}$ clusters to enable stable nitrogen reduction reaction (NRR) without significant structural degradation. The Au_{25}@S-G exhibits an ammonia yield rate of 27.5 $\mu g_{NH_3} \cdot mg_{Au}^{-1} \cdot h^{-1}$ at −0.5 V with faradic efficiency of 2.3%. More importantly, the anchored clusters preserve ~ 80% NRR activity after four days of continuous operation, a significant improvement over the 15% remaining ammonia production rate for clusters loaded on undoped graphene tested under the same conditions. Isotope labeling experiments confirmed the ammonia was a direct reaction product of N_2 feeding gas instead of other chemical contaminations. *Ex-situ* X-ray photoelectron spectroscopy and X-ray absorption near-edge spectroscopy of post-reaction catalysts reveal that the sulfur dopant plays a critical role in stabilizing the chemical state and coordination environment of Au atoms in clusters. Further ReaxFF molecular dynamics (RMD) simulation confirmed the strong interaction between Au nanoclusters (NCs) and S-G. This substrate-anchoring process could serve as an effective strategy to study ultrafine nanoclusters' electrocatalytic behavior while minimizing the destruction of the under-coordinated surface motif under harsh electrochemical reaction conditions.

KEYWORDS

gold nanoclusters, sulfur-doped graphene, nitrogen reduction reaction, electrocatalysis, anchoring effect

1 Introduction

The discrete electronic structure of small nanoclusters (NCs) (3–40 atoms) can lead to unique chemical and spectroscopic properties [1–4]. Moreover, because of the under-coordinated surface they can display unique chemisorption behaviors compared with conventional large nanoparticle systems (> 2 nm diameter) [5]. Thus the ultrafine (from sub-nanometer to ~ 2 nm) NCs have attracted growing interest for applications to such catalytic reactions, as selective hydrogenation [6], carbon dioxide reduction [7–9], and carbon monoxide oxidation [10]. However, the significant surface under-coordinating nature of NCs tends to induce the sintering and aggregation of the clusters with formation of larger particles during reaction, considerably altering the experimental size–reactivity relationship. Hence, a crucial challenge to exploit the intrinsic catalytic properties of NCs [11] is to achieve cluster stability.

Extensive studies have demonstrated that porous materials such as metal-organic framework (MOF) [12–14] and zeolite materials [15] can effectively interact and confine metallic clusters having just a few atoms. However, the low conductivity of these carrier materials prevents their use as electrochemical substrates. Moreover, for electrocatalytic systems Ostwald ripening can cause severe agglomeration and destruction of the NCs. Thus, an ideal substrate that can stabilize under-coordinated NCs in a harsh electrocatalysis environment should feature two critical characteristics:

1) good electrical conductivity that allows the electron transfer process;

2) strong anchoring capability to maintain the overall structure of ultrafine NCs.

It is well-established that Au forms relatively strong bond with sulfur atoms [16, 17]. Herein, we use sulfur-doped graphene (S-G) to demonstrate a dopant-anchoring strategy that can effectively stabilize the ultrafine $Au_{25}(PET)_{18}$ cluster (abbreviated as Au_{25} for simplicity) for long term electrocatalysis. The Au_{25}@S-G exhibits remarkable stability for the nitrogen reduction reaction (NRR) with a superior ammonia production rate. *Ex-situ* structural characterizations confirm that the morphology and chemical state of the ultrafine Au_{25} NCs are well maintained.

Address correspondence to p_yang@berkeley.edu

2 Experimental

2.1 Synthesis and isolation of $Au_{25}(PET)_{18}$

Neutral $Au_{25}(PET)_{18}$ NCs were prepared by a modified method from a previously reported protocol [18]. $HAuCl_4 \cdot 3H_2O$ (19.7 mg, 0.05 mmol) and tetraoctylammonium bromide (TOAB) (32.8 mg, 0.06 mmol) were dissolved in a round bottom flask with 5 mL of tetrahydrofuran. The solution was vigorously stirred for 15 min to form a dark red solution. Phenylethanethiol (PET) (34.5 mg, 0.25 mmol) was then added to the solution. A transparent solution was obtained after 30 min. $NaBH_4$ (18.9 mg, 0.5 mmol) was dissolved in 1 mL ice-cold water and added immediately to the reaction mixture. The reaction was stopped after 24 h. The crude sample was precipitated by a large excessive of ice-cold water and washed with methanol 3 times to remove unreacted precursors and free TOAB. The crude sample was passed through a silica column and subsequent size-exclusion column to yield pure neutral $Au_{25}(PET)_{18}$ NCs. The purity of the sample was confirmed by UV–vis, electrospray ionization mass spectrometry (ESI-MS) analysis, and ^1H NMR. The ultraviolet–visible (UV–vis) spectrum of $Au_{25}(PET)_{18}$ NCs shows the characteristic absorption at 402, 459, 639, and 693 nm. The ^1H NMR spectra of both TOAB and $Au_{25}(PET)_{18}$ were recorded. The NMR peaks of $Au_{25}(PET)_{18}$ are consistent with the reported spectrum, which differ from those of $[Au_{25}(PET)_{18}]^- \cdot TOAB^+$. The peaks of TOAB at 3.56(t), 2.41(s), 1.73(s), and 1.14(d) were not detected in $Au_{25}(PET)_{18}$, confirming the complete removal of TOAB in $Au_{25}(PET)_{18}$.

2.2 Physical characterizations

Transmission electron microscopy (TEM) was carried out using Hitachi H-7650. Inductively coupled plasma optical emission spectroscopy (ICP-OES) was tested using PerkinElmer Optima 7000 DV. X-ray photoelectron spectroscopy (XPS) (Thermo Scientific K-alpha) measurement was conducted using an Al Kα source.

2.3 Catalyst loading and electrode preparation

Purified $Au_{25}(PET)_{18}$ was dispersed in toluene solution and mixed with sulfur-doped graphene via vigorous stir (500 rpm) for 1 h. The Au_{25}@S-G was blow-dried by N_2. For electrode preparation, Au_{25}@S-G was dispersed in a mixture of ethanol and Nafion 117 solution (volume ratio of 100:1) with a concentration of 1 $mg_{catalyst} \cdot mL^{-1}$ to form catalyst ink. The catalysts ink was drop cast on carbon paper (0.5 cm × 2 cm) on both sides. The mass of loaded Au was measured by ICP-OES.

2.4 Electrochemical measurements

The NRR experiments were carried out using a three-electrode Nafion membrane-separated H-cell on a BioLogic potentiostat system. A graphite rod and Ag/AgCl (3 M KCl) were used as a counter electrode and a reference electrode, respectively. Note that both the Nafion membrane and graphite rod were pretreated in 5% H_2O_2 aqueous solution and ultrapure water at 80 °C for 2 h. 0.05 M H_2SO_4 was used as the electrolyte. Prior to NRR testing, the catalyst was activated by 20 potential cycles between −0.2 and 0.2 V in Ar-saturated electrolyte for activation. To remove the trace NH_3 impurity, ultrapure N_2 gas (99.99%) was bubbled through H_2SO_4 (1 M) aqueous solution before fed into the electrolyte. The electrolyte was saturated with N_2 for 30 min ahead of NRR experiments. During the NRR experiment, a constant N_2 flow (20 sccm) was fed into the electrolyte at the cathode side. All potentials were calibrated into values versus reversible hydrogen electrode (RHE) via hydrogen evolution reaction (HER)/hydrogen oxidation reaction (HOR) cyclic voltammetry (CV) scan using two platinum wires as working electrode (WE) and counter electrode (CE).

2.5 Determination of ammonia concentration

Indophenol blue method was used to determine the ammonia concentration in the electrolyte. The concentration of ammonia in the electrolyte was determined using the indophenol blue method with commercialized ammonia TNT830 vial test kit (Purchased from HACH). 5 mL electrolyte was added to the ammonia reagent vial. After inverting the cap, the vail was settled for 15 min before UV–vis spectra were collected. The NH_3 production was indicated by the formation of indophenol blue, which was determined by the absorbance at 680 nm, with its concentration calibrated by a standard plot using a series of standard ammonium sulfate solutions. NMR measurements were done on a Bruker Avance 500 system with water suppression.

2.6 Isotope experiment

$^{15}N_2$ isotopic experiment was performed using the same setup with the only change that the feeding gas was switched to $^{15}N_2$ gas. The cell was pre-purged with Ar for 30 min. The operation current at constant potential under $^{15}N_2$ was performed using the same potentiostat as above. The quantification of ammonia was accomplished by NMR of the post-reaction cathodic electrolyte.

3 Results and discussion

3.1 Synthesis and characterization ofAu_{25}NCs and Au_{25}@ S-G

We first synthesized $Au_{25}(PET)_{18}$ NCs via a conventional solution-phase method [18]. The synthesis protocol for NCs is illustrated in Fig. 1(a), with the experimental procedures detailed in Experimental Section in the Electronic Supplementary Material (ESM). The reaction time, temperature, and concentration of Au precursors were optimized to achieve good morphology and

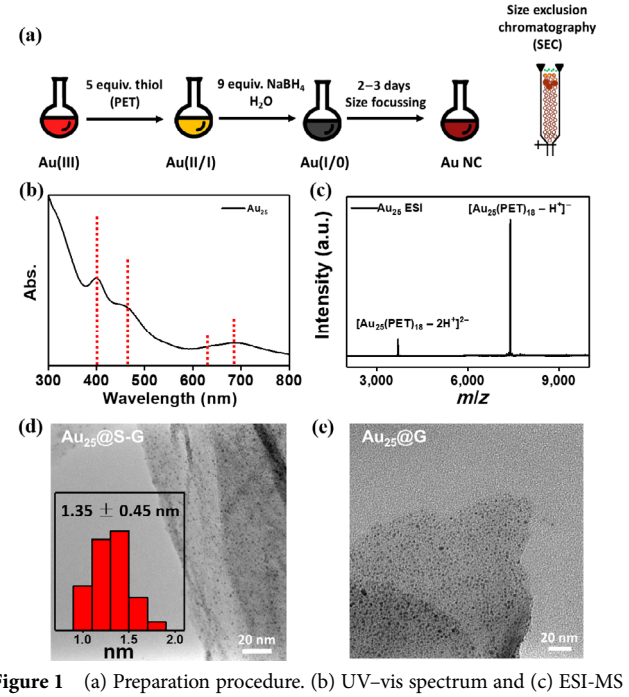

Figure 1 (a) Preparation procedure. (b) UV–vis spectrum and (c) ESI-MS of as-synthesized $Au_{25}(PET)_{18}$ clusters. Typical TEM images of $Au_{25}(PET)_{18}$ clusters loaded on (d) sulfur-doped graphene and (e) graphene. The inset histogram of (d) shows the size distribution.

uniformity. The as-synthesized Au clusters were purified by passing through a silica column and subsequent size-exclusion column to yield pure neutral $Au_{25}(PET)_{18}$ NCs. UV–vis spectroscopy and ESI-MS analysis were used to confirm the sample's purity. As shown in Fig. 1(b), the UV–vis spectrum of $Au_{25}(PET)_{18}$ NCs shows typical characteristic absorption peaks at 402, 459, 639, and 693 nm (highlighted with the red dashes in Fig. 1(b)), which agree with previous reported neutral $Au_{25}(PET)_{18}$ results [18]. ESI-MS results (Fig. 1(c)) confirm that the purified NCs are $Au_{25}(PET)_{18}$ with atomic monodispersity, and the isotopic distribution patterns are consistent with the simulated pattern of $Au_{25}(PET)_{18}$ (Fig. S1 in the ESM). ^1H NMR spectra (Fig. S2 in the ESM) confirm the complete removal of TOAB in $Au_{25}(PET)_{18}$.

To evaluate the stabilization capability of S-G, we used undoped graphene nanoplatelets (G) as a reference substrate for comparison. After purification of Au_{25}, the loading process was conducted by stir-mixing NCs and supporting materials in toluene at room temperature (RT) for 1 h. TEM shows the overall size and uniformity of as-loaded Au_{25}. As shown in Fig. 1(d), Au_{25} NCs are uniformly distributed on S-G with an ultrafine average size of 1.35 ± 0.45 nm based on statistical analysis (inset of Fig. 1(d)). In contrast, NCs loaded on graphene substrates show a significant trend toward aggregation. Nanoparticles with sizes ranging from 2 to 4 nm could be readily identified on the TEM image (Fig. 1(e)). This aggregating phenomenon on graphene can be attributed to the lack of interacting species. $Au_{25}(PET)_{18}$ can interact with the substrate only via π–π conjugation between the PET staple ligand and graphene.

3.2 The electrocatalytic NRR tests of Au_{25}@S-G and Au_{25}@G

We performed NRR in 0.05 M H_2SO_4 electrolyte to evaluate the electrocatalytic property and stability of the Au_{25}@S-G composites. Au mass loading was determined to be to 11 $\mu g \cdot cm^{-2}$ for both Au_{25}@S-G and Au_{25}@G (confirmed by inductively coupled plasma mass spectrometry). A graphite rod and an Ag/AgCl (WPI, 3M KCl) electrode were used as a counter electrode and a reference electrode, respectively. The ammonia yield rate was determined by the UV–vis absorption spectra of the electrolyte stained with a commercial indophenol indicator (TNT830) after 3 h NRR operations under various electrochemical potentials. The concentration of NH_4^+ in the electrolyte was calibrated by a commercial standard ammonia solution. The standard plot shows a highly linear relationship between absorbance and concentration (Figs. S3(a)–S3(c) in the ESM). As shown in Fig. 2(a), Au_{25}@S-G exhibits a peak NH_3 yield rate of 27.5 $\mu g_{NH_3} \cdot mg_{Au}^{-1} \cdot h^{-1}$ at −0.5 V with a faradic efficiency (FE) of 2.3%. This Au mass-normalized production rate is among the highest for previously reported Au-based NRR electrocatalysts [19–21]. When the operation potential is made more negative, both the ammonia production rate and the FE drop dramatically due to the competing HER. As background reference, the NRR catalytic test with S-G alone shows negligible ammonia yield under the same electrochemical testing condition (Figs. S4(a) and S4(b) in the ESM). High-angle annular dark-field scanning transmission electron microscopy (HAADF-STEM) (Figs. 2(b) and 2(c)) was used to monitor the morphology change between pristine Au_{25} and post-NRR Au_{25}. In this side-by-side comparison, the size and distribution of NCs on S-G remain mostly unchanged after 3 h of NRR operation. The blurred substrate in the STEM image (Fig. 2(c)) was induced by the addition of Nafion when preparing the electrode.

To detect trace amounts of ammonia, quantitative isotope measurement is needed to rule out potential contamination from the surrounding environment [22]. We conducted $^{15}N_2$ isotope labeling experiments to confirm that the nitrogen species in NH_4^+ generated came from the N_2 feed gas (Figs. S5(a)–S5(c) in the ESM). We note that a set of tiny $^{14}NH_4^+$ background triplet peaks appear in the NMR spectra (Fig. S5(c) in the ESM). These peaks could be attributed to the 2%–3% $^{14}N_2$ impurity in the $^{15}N_2$ isotope gas tank from the vendor.

Stability tests of Au_{25}@S-G and Au_{25}@G were conducted by chronoamperometry (CA) with operation potentials at −0.3 V vs. RHE. The tests were paused every 24 h to analyze ammonia concentration in the catholyte, and the electrolyte was refreshed before resuming operation. The initial NRR activity of Au_{25}@S-G was 9.5 $\mu g_{NH_3} \cdot mg_{Au}^{-1} \cdot h^{-1}$ at −0.3 V with a FE of 4.9%, while Au_{25}@G exhibited 2.28 $\mu g_{NH_3} \cdot mg_{Au}^{-1} \cdot h^{-1}$ catalytic activity at −0.3 V with a FE of 1.85%. The ammonia production rate (R) was normalized by the initial rate ($R_{initial}$) at different times to compare the trend in stability. As shown in Fig. 2(d), the NH_3 yield rate for Au_{25}@S-G drops ~ 4% per day for the first 96 h. In contrast, a dropping rate of ~ 20% activity was observed for the Au_{25}@G sample. TEM characterizations of post-test samples show that S-G supported NCs (Fig. 2(e)) maintain impressive dispersity and morphology even after 96 h catalytic operation. Whereas Au_{25}@G (Fig. 2(f)) leads to NCs suffering from severe

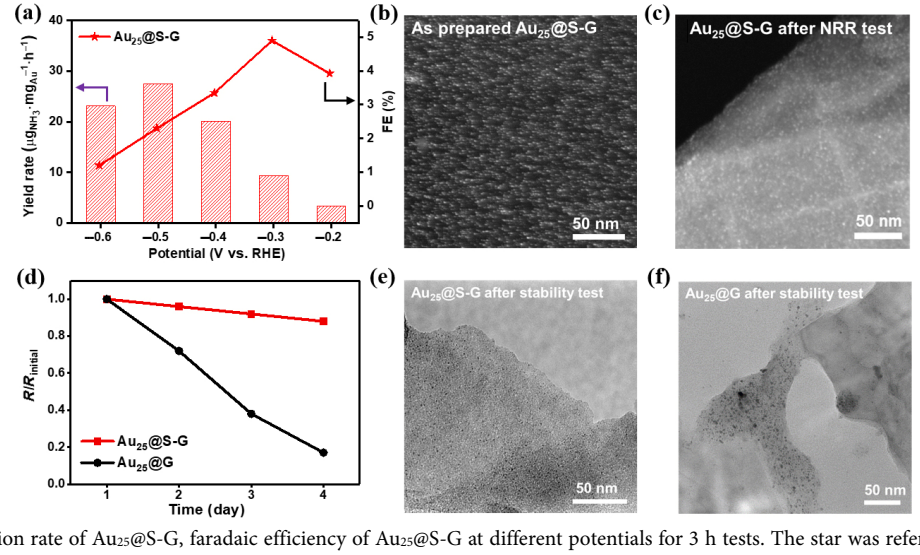

Figure 2 (a) Production rate of Au_{25}@S-G, faradaic efficiency of Au_{25}@S-G at different potentials for 3 h tests. The star was referring to the FE, and the histogram represents the ammonia yield rate. HAADF-STEM images of the (b) as-prepared Au_{25}@S-G and (c) Au_{25}@S-G post electrolysis in 0.05 M H_2SO_4 at −0.3 V for 3 h. (d) Stability test of Au_{25}@S-G and Au_{25}@G, respectively. TEM images of (e) Au_{25}@S-G and (f) Au_{25}@G post 96 h NRR stability test.

agglomeration in the post durability test.

3.3 The origin of the enhanced stability of Au_{25}@S-G configuration

Ex-situ XPS was used to probe the chemical state of Au species after interacting with the sulfur-doped substrate. The XPS result for pristine Au_{25} NCs (Fig. 3(a)) shows that the chemical state of Au in pristine clusters is predominately Au^0, which is consistent with previous spectroscopy studies [23–24]. After loading the NCs on S-G, the XPS of the Au_{25}@S-G composite shows increasing Au^{x+} peaks with a binding energy of 86 and 89.6 eV for the Au 4f core-level region (labeled as a blue dot in Fig. 3(b)), which we attribute to the interaction between the sulfur dopant on S-G with Au_{25} NCs. After conducting NRR at −0.3 V for 3 h, the XPS for the post-reaction Au_{25}@S-G shows a slightly increased Au^{x+} ratio (Fig. 3(c)) compared with as-loaded NCs. This result indicates that the chemical state of the Au NCs is stable during catalytic operation, reflecting a strong interaction between sulfur dopant and NCs.

To investigate the interaction mechanism and to probe the local Au atomistic and electronic structure, we conducted extended X-ray absorption fine structure (EXAFS) and X-ray absorption near-edge structure (XANES) measurements on Au_{25}@S-G and Au_{25}@G post 3 h NRR tests at −0.3 V vs. RHE. We use white line intensity to probe the oxidation state of Au at the Au L-edge in XANES spectra. The Au XANES result shows that the white line intensities of both samples (Fig. 3(d)) are close to that of an Au foil, indicating that the average oxidation state of the NCs is close to a metallic state. The Au EXAFS (Fig. 3(e)) fitting results show an Au–Au bond length of 2.83 Å with coordination number (CN) = 1.1 (Table S1 in the ESM) for Au_{25}@S-G samples, which is in line with the value for pure Au_{25} and for the predicted Au_{13} icosahedral core group (Au–Au bond length 2.78, CN 1.44) in a previous structural study [25]. Moreover, both Au_{25}@S-G and Au_{25} show a Au–S bond length of 2.32 Å with similar Au–S CN (1.8 of Au_{25}@S-G and 1.9 of Au_{25}). Combined with our XPS result, we conclude that the sulfur dopant on S-G partially replaces the thiol ligand to bind with outer Au atoms. This result also demonstrates that the Au_{25}@S-G can maintain the coordination characteristics of $Au_{25}(PET)_{18}$ even after the catalytic process.

In contrast, the EXAFS result for Au_{25}@G shows an Au–Au bond length 2.86 with CN of 4.1 post NRR, indicating that aggregation has caused Au_{25} to lose cluster characteristics, getting closer to the bulk system. Additionally, comparing Au_{25}@S-G with pristine Au_{25}, the decreased Au–S coordination number (1.5 of Au_{25}@G vs. 1.8 of Au_{25}@S-G and 1.9 of Au_{25}) is plausible due to the ligand loss during sintering. This result shows that the monodispersed nanoclusters without anchoring species on graphene aggregate during a dynamic electrocatalytic process.

To further reveal the sulfur-dopant role in stabilizing Au NCs, we carried out atomistic simulations using the reactive force field (ReaxFF). Based on the experimental results, we constructed two optimized models for computation study: 1) $Au_{25}(PET)_{18}$ on graphene (Fig. 4(a)); 2) $Au_{25}(PET)_{18}$ on sulfur-doped graphene, with one ligand on the cluster replaced by a sulfur-dopant (Fig. 4(b)). We calculated the binding energies of the two structures (Table S2 in the ESM), finding a binding energy of 2.23 eV for Au_{25}@G, and a binding energy of 7.11 eV for Au_{25}@S-G. Therefore, the interaction of Au NCs with S-G is 4.88 eV stronger, consistent with experimental observations. More importantly, this stronger interaction will help prevent cluster aggregation. To prove this point, we carried out molecular dynamics simulations for Au_{25} dimers on these surfaces, at

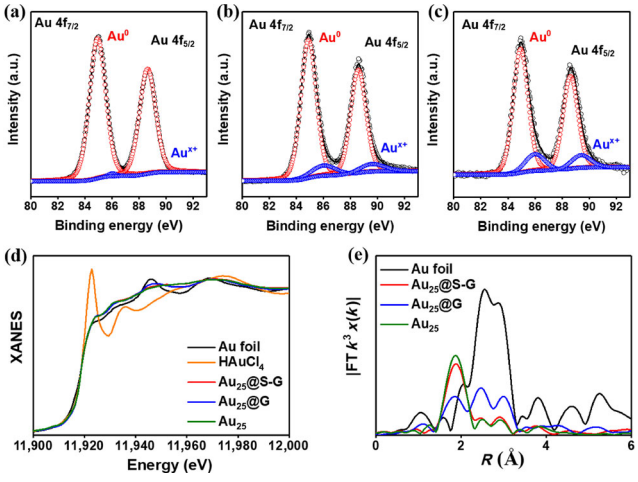

Figure 3 XPS of (a) as-synthesized $Au_{25}(PET)_{18}$ clusters, (b) as-loaded Au_{25}@S-G and (c) Au_{25}@S-G post NRR test. (d) XANES and (e) Au L_3 edge FT-EXAFS of Au_{25}@S-G and Au_{25}@G post 3 h NRR test at −0.3 V vs. RHE, with Au foil and $Au_{25}(PET)_{18}$ as the references.

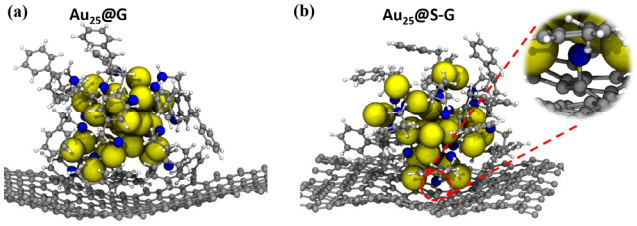

Figure 4 Results from 2 ns RMD simulations followed by geometry optimization. Snapshots of (a) $Au_{25}(PET)_{18}$ on graphene and (b) $Au_{25}(PET)_{18}$ on sulfur-doped graphene, with one ligand on cluster replaced by sulfur-dopant after anchoring.

298 K for 2 ns. The simulation results (Movies ESM1 and ESM2) show that in 2 ns of ReaxFF molecular dynamics (RMD) simulation, sintering occurs for Au_{25}@G, but not for Au_{25}@S-G model (Fig. S6 in the ESM). This shows that the enhanced binding can indeed play a role in stabilizing the Au NCs. These two observations are of the most importance in promoting catalysis performance and stability.

4 Conclusion

In conclusion, we successfully demonstrated that sulfur-doped graphene can stabilize ultrafine Au clusters for long term NRR electrocatalysis. The Au_{25}@S-G catalysts exhibit a high ammonia production rate of 27.5 $\mu g_{NH_3} \cdot mg_{Au}^{-1} \cdot h^{-1}$ with a FE of 2.3% at −0.5 V. More importantly, the NCs maintain an 80% NRR yield rate after the 96 h stability test without morphology destruction. *Ex-situ* TEM and STEM characterizations highlight the remarkable structural stability of the Au_{25}@S-G composite. XPS and EXAFS studies support the stabilized chemical state and coordination status of NCs after interacting with S-G. It would be interesting to extend this work, to consider substrates with other chemical dopants (e.g., N, P) to be utilized as an anchoring platform to probe the ultrafine NC intrinsic electrocatalytic behavior. This study may contribute to bridge the gap between conventional nanoparticles [20, 21] and molecular single atomic catalysts [19], to provide electrocatalytic mechanism insight about ultrafine NCs.

Acknowledgements

This research was supported by the Director, Office of Science, Office of Basic Energy Sciences, Chemical Sciences, Geosciences,

& Biosciences Division, of the US Department of Energy under Contract DEAC02-05CH11231, FWP CH030201 (Catalysis Research Program). The Advanced Light Source was supported by the Director, Office of Science, Office of Basic Energy Sciences, of the US Department of Energy under Contract DE-AC02-05CH11231. This work made use of the facilities at the NMR Facility, College of Chemistry, University of California, Berkeley. Inductively coupled plasma optical emission spectrometry was supported by the Microanalytical Facility, College of Chemistry, University of California, Berkeley. Part of this material (WAG, TC) was based on work performed by the Liquid Sunlight Alliance, which was supported by the US Department of Energy, Office of Science, Office of Basic Energy Sciences, Fuels from Sunlight Hub under Award Number DE-SC0021266.

This work is dedicated to the occasion of 80th birthday for Prof. Yitai Qian. As the undergraduate advisor for one of the authors (P. D. Y.), Prof. Qian has had profound impact on this author's career in the field of materials chemistry. P. D. Y. would like to acknowledge the unconditional support, encouragement and guidance from Prof. Qian back in the early 1990s. It was during that time P. D. Y. started his journey in solid state chemistry, by working on high temperature cuprate superconductors and finishing his undergraduate thesis on this exciting topic. The title page of this thesis was attached here (dated June 10, 1993).

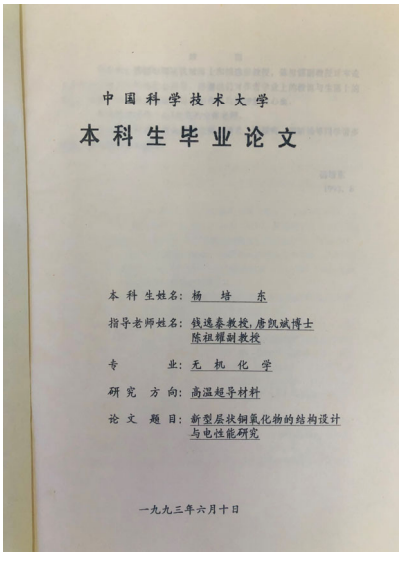
中国科学技术大学

本科生毕业论文

本科生姓名：杨 培 东

指导老师姓名：钱逸泰教授，唐凯斌博士
陈祖耀副教授

专 业：无 机 化 学

研究方向：高温超导材料

论文题目：新型层状铜氧化物的结构设计与电性能研究

一九九三年六月十日

Electronic Supplementary Material: Supplementary material (further details of the EXAFS fitting, computational method, ^{1}H NMR for purified $Au_{25}PET_{18}$ clusters, UV–vis calibration curves for ammonia determination, isotope labeling NMR result, and optimized coordinates for simulation model) is available in the online version of this article at https://doi.org/10.1007/s12274-021-3561-2.

References

[1] Liu, L. C.; Corma, A. Metal catalysts for heterogeneous catalysis: From single atoms to nanoclusters and nanoparticles. *Chem. Rev.* **2018**, *118*, 4981–5079.

[2] Liu, L. C.; Corma, A. Confining isolated atoms and clusters in crystalline porous materials for catalysis. *Nat. Rev. Mater.* **2021**, *6*, 244–263.

[3] Taylor, K. J.; Pettiette-Hall, C. L.; Cheshnovsky, O.; Smalley, R. E. Ultraviolet photoelectron spectra of coinage metal clusters. *J. Chem. Phys.* **1992**, *96*, 3319–3329.

[4] Kelly, K. L.; Coronado, E.; Zhao, L. L.; Schatz, G. C. The optical properties of metal nanoparticles: The influence of size, shape, and dielectric environment. *J. Phys. Chem. B* **2003**, 107, 668–677.

[5] Buceta, D.; Piñeiro, Y.; Vázquez–Vázquez, C.; Rivas, J.; López–Quintela, M. A. Metallic clusters: Theoretical background, properties and synthesis in microemulsions. *Catalysts* **2014**, *4*, 356–374.

[6] Zhu, Y.; Qian, H. F.; Drake, B. A.; Jin, R. C. Atomically precise $Au_{25}(SR)_{18}$ nanoparticles as catalysts for the selective hydrogenation of α,β-unsaturated ketones and aldehydes. *Angew. Chem., Int. Ed.* **2010**, *122*, 1317–1320.

[7] Zhang, H.; Liu, H.; Tian, Z. Q.; Lu, D.; Yu, Y.; Cestellos-Blanco, S.; Sakimoto, K. K.; Yang, P. D. Bacteria photosensitized by intracellular gold nanoclusters for solar fuel production. *Nat. Nanotech.* **2018**, *13*, 900–905.

[8] Austin, N.; Zhao, S.; McKone, J; Jin, R.; Mpourmpakis, G. Elucidating the active sites for CO_2 electroreduction on ligand-protected Au_{25} nanoclusters. *Catal. Sci. Technol.* **2018**, *8*, 3795–3805.

[9] Kauffman, D. R.; Thakkar, J.; Siva, R.; Matranga, C.; Ohodnicki, P. R.; Zeng, C. J.; Jin, R. C. Efficient electrochemical CO_2 conversion powered by renewable energy. *ACS Appl. Mater. Interfaces* **2015**, *7*, 15626–15632.

[10] Kim, H. Y.; Lee, H. M.; Henkelman, G. Co oxidation mechanism on CeO_2-supported Au nanoparticles. *J. Am. Chem. Soc.* **2012**, *134*, 1560–1570.

[11] Zhang, B.; Chen, C. B.; Chuang, W.; Chen, S. P.; Yang, P. D. Size transformation of the $Au_{22}(SG)_{18}$ nanocluster and its surface-sensitive kinetics. *J. Am. Chem. Soc.* **2020**, *142*, 11514–11520.

[12] Vilhelmsen, L. B.; Walton, K. S.; Sholl, D. S. Structure and mobility of metal clusters in MOFs: Au, Pd, and AuPd clusters in MOF-74. *J. Am. Chem. Soc.* **2012**, *134*, 12807–12816.

[13] Dou, L.; Wu, S. N.; Chen, D. L.; He, S. H.; Wang, F. F.; Zhu, W. D. Structures and electronic properties of Au clusters encapsulated ZIF-8 and ZIF-90. *J. Phys. Chem. C* **2018**, *122*, 8901–8909.

[14] Li, J. P.; Wang, W. Y.; Chen, W. X.; Gong, Q. M.; Luo, J.; Lin, R. Q.; Xin, H. L.; Zhang, H.; Wang, D. S.; Peng, Q. et al. Sub-nm ruthenium cluster as an efficient and robust catalyst for decomposition and synthesis of ammonia: Break the "size shackles". *Nano Res.* **2018**, *11*, 4774–4785.

[15] Liu, L. C.; Díaz, U.; Arenal, R.; Agostini, G.; Concepción, P.; Corma, A. Generation of subnanometric platinum with high stability during transformation of a 2D zeolite into 3D. *Nat. Mater.* **2017**, *16*, 132–138.

[16] Häkkinen, H. The gold–sulfur interface at the nanoscale. *Nat. Chem.* **2012**, *4*, 443–455.

[17] Bürgi, T. Properties of the gold–sulphur interface: From self-assembled monolayers to clusters. *Nanoscale* **2015**, *7*, 15553–15567.

[18] Kauffman, D. R.; Alfonso, D.; Matranga, C.; Qian, H. F.; Jin, R. C. Experimental and computational investigation of Au_{25} clusters and CO_2: A unique interaction and enhanced electrocatalytic activity. *J. Am. Chem. Soc.* **2012**, *134*, 10237–10243.

[19] Qiu, Y.; Peng, X. Y.; Lü, F.; Mi, Y. Y.; Zhuo, L. C.; Ren, J. Q.; Liu, X. J.; Luo, J. Single-atom catalysts for the electrocatalytic reduction of nitrogen to ammonia under ambient conditions. *Chem.—Asian J.* **2019**, *14*, 2770–2779.

[20] Wang, H. J.; Yu, H. J.; Wang, Z. Q.; Li, Y. H.; Xu, Y.; Li, X. N.; Xue, H. R.; Wang, L. Electrochemical fabrication of porous Au film on Ni foam for nitrogen reduction to ammonia. *Nano Micro Small* **2019**, *15*, 1804769.

[21] Liu, D.; Zhang, G.; Ji, Q. H.; Zhang, Y. Y.; Li, J. H. Synergistic electrocatalytic nitrogen reduction enabled by confinement of nanosized Au particles onto a two-dimensional Ti_3C_2 substrate. *ACS Appl. Mater. Interfaces* **2019**, *11*, 25758–25765.

[22] Andersen, S. Z.; Čolić, V.; Yang, S.; Schwalbe, J. A.; Nielander, A. C.; McEnaney, J. M.; Enemark-Rasmussen, K.; Baker, J. G.; Singh, A. R.; Rohr, B. A. et al. A rigorous electrochemical ammonia synthesis protocol with quantitative isotope measurements. *Nature* **2019**, *570*, 504–508.

[23] Zhang, P. X-ray spectroscopy of gold-thiolate nanoclusters. *J. Phys. Chem. C* **2014**, *118*, 25291–25299.

[24] Mathew, A.; Varghese, E.; Choudhury, S.; Pal, S. K.; Pradeep, T. Efficient red luminescence from organic-soluble Au_{25} clusters by ligand structure modification. *Nanoscale* **2015**, *7*, 14305–14315.

[25] MacDonald, M. A.; Chevrier, D. M.; Zhang, P.; Qian, H.; Jin, R. The structure and bonding of $Au_{25}(SR)_{18}$ nanoclusters from EXAFS: The interplay of metallic and molecular behavior. *J. Phys. Chem. C* **2011**, *115*, 15282–15287.